Hindawi
Geofluids
Volume 2021, Article ID 4720242, 11 pages
https://doi.org/10.1155/2021/4720242

Research Article

A New Method Based on Boundary Element Method to Appraise CO_2 Geological Storage Potential in Depleted Shale Gas Reservoirs

Junjie Shi,[1] **Linsong Cheng**,[1] **Chong Cao**,[1] **Renyi Cao**,[1] **Deqiang Wang**,[2] **and Gaoling Liu**[3]

[1]*College of Petroleum Engineering, China University of Petroleum, Beijing. Beijing, China 102249*
[2]*State Key Laboratory of Oil Offshore Exploration (CNOOC Research Institute), Beijing, China 100020*
[3]*PipeChina Oil and Gas Control Center, Beijing, China 100020*

Correspondence should be addressed to Linsong Cheng; 996757751@qq.com and Renyi Cao; caorenyi@cup.edu.cn

Received 18 April 2021; Revised 4 August 2021; Accepted 11 August 2021; Published 17 September 2021

Academic Editor: Hamed Lamei Ramandi

In recent years, greenhouse gases have increased in the atmosphere, and climate change concerns have triggered global efforts to find solutions for CO_2 capture, separation, transport, and storage. Geological sequestration in the depleted unconventional reservoir is an effective measure to reduce the atmosphere's CO_2 content. The exact evaluation of the CO_2 storage capacity can verify the feasibility of storing carbon dioxide and parameter optimization. A reasonable boundary element method to estimating the CO_2 storage capacity of depleted shale gas reservoirs considering arbitrarily shaped boundaries is introduced. Firstly, the physical model with fracture networks is built based on the microseismic data. Then, the flow equation including the matrix and fracture can be obtained considering adsorption, and the star-delta transformation is used to deal with interconnected fracture segments. The point source function with an infinite boundary can be obtained after the Laplace transform method. Finally, the semianalytical flow solution is obtained by using the boundary element method in the Laplace region. Moreover, the results have a high agreement with commercial software for the regular boundary. The sensitivity of relevant parameters is analyzed by this method, and the importance of considering the boundary shape is emphasized. This method can evaluate the CO_2 storage capacity of formation with the irregular boundary and is regarded as the guide of parameter optimization in CO_2 storage.

1. Introduction

Greenhouse gases such as CO_2 have increased in the atmosphere leading to climate change concerns [1]. Global efforts have been made to reduce atmospheric CO_2 concentration by carbon sequestration, including geological sequestration, mineral carbonation, and ocean storage [2]. Furthermore, the CO_2 geological sequestration is a widely applied measure. Industrial analogs, including natural gas and acid gas injection projects, have proved that CO_2 can be safely injected and stored [3].

The gas injection into the reservoirs is widely used in petroleum engineering to enhance oil recovery, and it is feasible to store CO_2 in geological formations as a CO_2 reduction option [4]. In the beginning, most research on gas injection for improving oil recovery takes a typical block as an example, which is based on the black oil numerical simulation with less consideration on the mechanism. In 2009, Shoaib and Hoffman first conducted mathematical modeling studies on enhanced recovery by CO_2 flooding and CO_2 injection huff-n-puff based on the Elm Coulee field (0.01-0.04 mD) block Bakken unconventional reservoir [5]. Wan et al. studied the influence of the stimulated reservoir volume (SRV) characteristics on the gas injection and huff-n-puff by numerical simulation, including the size of the SRV, fracture space, and stress sensitivity [6].

The research combined with the gas flooding mechanism in the experimental study and the component model was introduced to consider the miscibility based on the actual block data. Alharthy et al. [7] established a numerical model of gas injection stimulation and predicted the production rate of a horizontal well after volume fracturing in the field, which is based on the flow mechanism of CO_2 injection in the tight matrix proposed by Hawthorne et al., including the diffusion effect caused by crude oil expansion, viscosity reduction, and concentration difference [8]. Wan et al. [9] and Pu [10] established the component model about the gas huff-n-puff model considering the miscibility of crude oil and injected gas and carried out a numerical simulation study on enhanced oil recovery in the SRV region. Yu et al. [11] and Zhu et al. [12] used the component model to analyze the sensitivity of each influencing factor of gas flooding. Many numerical methods coupling business software are increasingly used due to advantages considering mechanism in the study of CO_2-EOR simulation [13]. Zuloaga-Molero et al. [14] applied an EDFM (embedded discrete fracture model) to build a compositional reservoir model investigating the effects on CO_2 huff-n-puff and CO_2 continuous injection, including complex fracture geometries, CO_2 diffusion, permeability, and natural fractures. Sun et al. [15] applied the proposed fracture discretization approach to CO_2 huff-n-puff in complex fracture and obtained more accurate simulation results than the dual continuum approach.

Some scholars proposed that saline aquifers can be a good storage site because of their vast volumes. However, oil and gas reservoirs also are suitable for storage, and the geological conditions and storage scale are explicit in the oil and gas exploration. On the other hand, the production well and injection well can be used as carbon dioxide injection devices, which can significantly reduce the cost of remake injection equipment [16]. The depleted shale reservoir is very promising compared to the deep saline aquifer [17]. The depleted shale gas reservoir is a good choice for CO_2 storage because of its tight pore space as both a storage reservoir and a seal [18]. First, the CO_2 could sorb into the nanoscale pore structure and be immobilized within the shale reservoir rock [19], which is an additional trapping mechanism compared to those in the deep saline aquifers. Besides, large volumes of CO_2 could be emplaced in the fracture network formation [20]. Moreover, their extremely tight pore in the shale formations indicates that they are less likely than saline aquifers to leak CO_2 [18]. Godec et al. [21] suggested that the economic estimate is predicted to be 71 Tcm of enhanced methane recovery, facilitating 280 Gt of CO_2 storage in gas shales globally. In addition, some physical simulation results also show that the depleted shale reservoir for CO_2 storage is effective and feasible. Busch et al. [22] provide evidence that shale has significant CO2 storage capacity through diffusion experiments and adsorption experiments. Arif et al. [23] made wettability experiments. The conclusions are that the shale with low TOC is suitable to be used as a typical caprock, and when the TOC content is higher than 1.1 wt%, the shale reservoir can trap a large amount of CO_2 gas by adsorption. As a potential CO_2 storage sites, it is meaningful and essential to precisely evaluate the depleted shale gas reservoir capacity.

CO_2 storage projects include depleted oil and gas reservoirs and saline aquifers, unmineable coal seams [17]. The research about depleted oil and gas reservoir evaluation method can be divided into the volume- or production-based calculation method, numerical simulation method, and semianalytical model method [24]. The volume- or production-based calculation method proposes the method based on original gas in place to calculate the storage volume previously occupied by gas and oil, which can be replaced by CO_2 [25, 26]. Kang et al. [27] and Tian et al. [28] estimated the reservoir capacity through rock samples' storage capacity and the overall reservoir volume. Abuov et al. [29] estimated effective CO_2 storage capacities in oil reservoirs, gas reservoirs, and saline aquifers for basins of Kazakhstan using the Carbon Sequestration Leadership Forum (CSLF) and United States Department of Energy (USDOE) methods. For the numerical simulation method, Ren and Duncan [28] discussed the effects of both injection strategies and reservoir heterogeneity on CO_2 storage by reservoir simulation of carbon storage associated with CO_2 EOR in residual oil zones in San Andres formation of West Texas Evgeniy. Their research showed that hydraulically fractured shale formations can be regarded as reservoirs for carbon dioxide sequestration. Andersen and Nilsen [30] evaluated CO_2 storage numerical simulation with thermal effects considering fluid properties and geomechanical stresses and the rate of geochemical reactions caused by temperature change around the injection well. Lashgari et al. [31] used CMG-GEM software to build a field-scale numerical simulation model to analyze the important physical mechanisms (miscibility and CO_2 adsorption, along with gas diffusion) of CO_2 storage and EOR. Liu et al. [32] evaluated the CO_2 sequestration ability of shale under three-dimensional complex geological conditions using a projection-based embedded discrete fracture model. For the semianalytical model method, many scholars study the CO_2 storage process using the semianalytical method by Laplace transformation, source function, and numerical discretion. Chen et al. [33, 34] developed a quick analytical method for estimating the CO_2 storage capacity of depleted shale gas based on pressure transient analysis (PTA). Xiao et al. [24, 35] quantitatively determined the abandonment pressure and analyze related impacts of dynamic parameters on it. Volume-based calculation methods simplified the CO_2 flow behavior and injection rate. Furthermore, the numerical simulation method needs modeling and mesh subdivision to apply to the field scale, which is time consuming. Semianalytical methods are suitable for rectangular or circular boundaries. However, there are few works that discussed the irregular boundary of formation. Therefore, it is vital to find efficient and convenient methods to consider the irregular boundary of formation.

Water in the shale will reduce the storage capacity due to gas-liquid two-phase flow and the occupied water volume. Moreover, the CO_2-water-shale reaction has implications for CO_2 flow [36]. Chen et al. [33, 34] evaluate the depleted shale CO_2 storage capacity by a single-phase flow for more convenient and quick evaluation. Similarly, Myshakin et al.

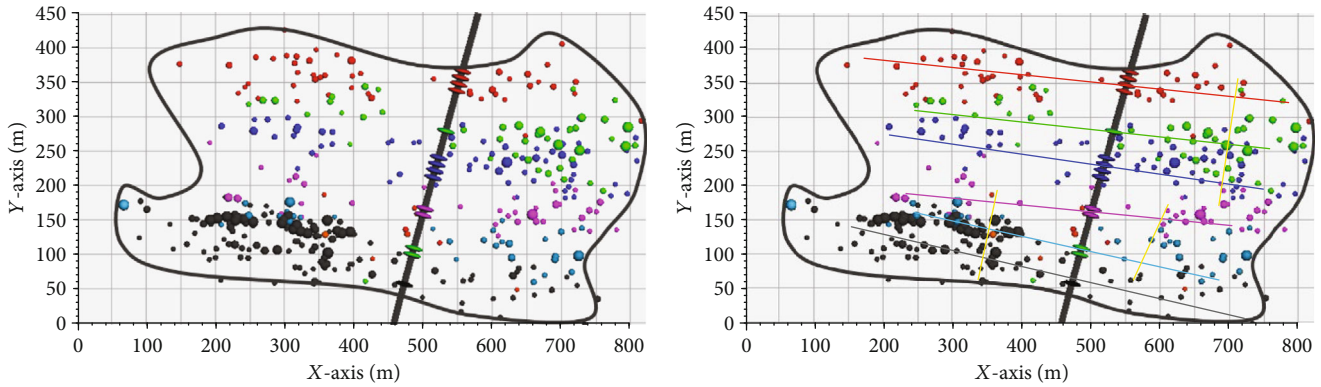

Figure 1: (a) The microseismic detection diagram. (b) The fracture network explained by the microseismic detection.

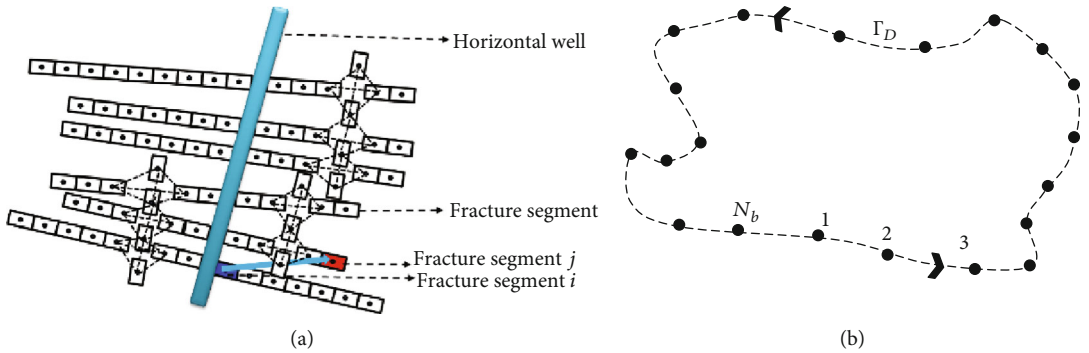

Figure 2: (a) Schematic of the discrete fracture model. (b) Schematic of discrete boundary.

[37] only consider CO_2 flow, single-phase flow, to evaluate flow regimes and storage efficiency. So the model is simplified to derive a semianalytical single-phase flow solution with the complex boundary in this paper. The semianalytical solution evaluation is carried out under relatively ideal conditions.

The boundary element method (BEM) has been used widely in fluid mechanics, fracture mechanics, and contact mechanics to solve linear partial differential equations formulated as integral equations. Many scholars have applied and modified the BEM into petroleum and environmental engineering [38–40]. The production and pressure calculation in forming the irregular boundary can be solved by BEM [41, 42].

A quick and reasonable boundary element method for estimating CO_2 storage capacity of depleted shale gas formation considering arbitrarily shaped boundaries is introduced in this paper. This physical model is built based on the microseismic data, and BEM solves the mathematical model. The star-delta transformation deals with interconnected fracture segments, and the results have a high agreement with commercial software for the regular boundary. Furthermore, a real case with a horizontal well after large-scale hydraulic fracturing in depleted shale gas reservoirs is discussed. The influence of injection pressure, stress sensitivity coefficient, fracture permeability, and shale matrix permeability on the storage capacity was studied.

2. Methodology for Estimating CO_2 Storage Potential

2.1. Physical Model. Microseismic detection is used widely to analyze the underground situation, which is shown in Figure 1(a). There is a microseismic map, which uses acoustic signals to determine the underground fractures. The same color points represent the same fracture, and the dense colored dots indicate fractures. Therefore, fracture networks consist of hydraulic and secondary fractures, explained and derived by microseismograms shown as Figure 1(b). The black straight line represents the horizontal well, and the area within the black curve represents the stimulated reservoir volume (SRV). It can be seen that the SRV with irregular boundaries has hydrofractures to easily inject gas, which can be used as a CO_2 storage place.

2.2. Mathematics Model and Solution. Figure 1(b) provides a schematic diagram of the horizontal well after large-scale hydraulic fracturing. The stimulated reservoir volume region shape is irregular. The following assumptions are provided:

(1) Only isothermal single-phase flow exists

Table 1: Reservoir parameters and production parameters (data from the literature [24]).

Reservoir parameters	Value
Abandonment pressure (MPa)	1.5
Formation temperature (K)	333
Horizontal length (m)	1000
Formation thickness (m)	15
Total compressibility of natural fracture (MPa^{-1})	5.0×10^{-4}
Total compressibility of the matrix (MPa^{-1})	4.5×10^{-4}
Total compressibility of hydraulic fracture (MPa^{-1})	5.0×10^{-4}
Porosity of natural fracture (-)	0.001
Porosity of matrix (-)	0.08
Porosity of hydraulic fracture (-)	0.3
Initial permeability of natural fracture (mD)	0.1
Permeability of matrix (mD)	5×10^{-3}
Permeability of hydraulic fracture (mD)	5000
Hydraulic fracture width (m)	0.003
Hydraulic fracture number (-)	4
CO_2 Langmuir pressure (MPa)	8
CO_2 Langmuir volume (sm^3/m^3)	8
Gas diffusion coefficient D (m^2/s)	0.0001

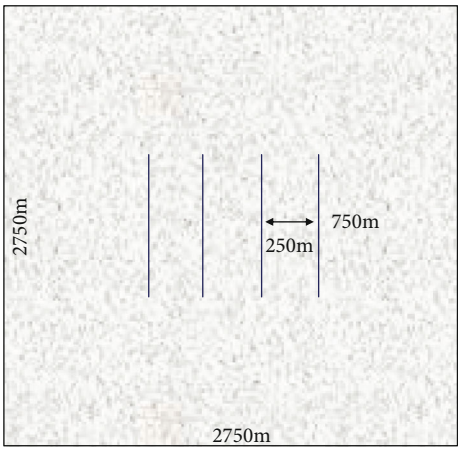

Figure 3: Schematic diagram of the physical model.

(2) The SRV is a dual porosity continuum medium. Gas flows only from the matrix system into the fracture system

(3) The gas flowing into the well from the formation is only caused by hydraulic fractures

(4) CO_2 adsorbs in the reservoirs following the Langmuir isothermal adsorption law. The adsorption only exists in the matrix system [33, 34].

(5) Hydraulic fractures and secondary fractures are infinite conductivity fractures

(6) Gravity and capillary forces were ignored in the study

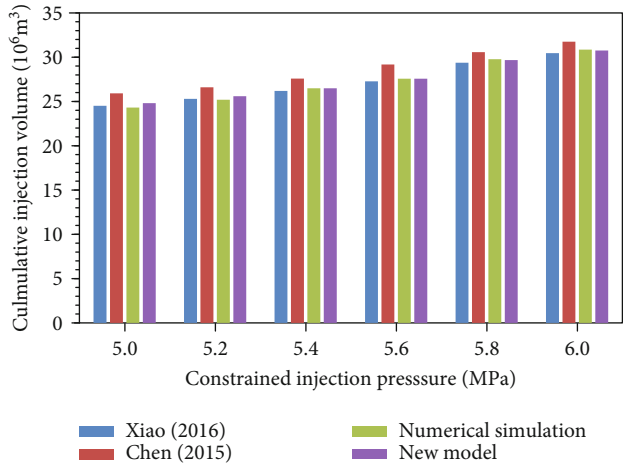

Figure 4: Validation of new proposed model: injection rate Q_{in} 100,000 m^3/d, injection time 365 days.

Table 2: Reservoir parameters and production parameters.

Reservoir parameters	Value
Abandonment pressure (MPa)	1.5
Matrix porosity (-)	0.092
Matrix permeability (mD)	5×10^{-3}
Hydraulic fracture porosity (-)	0.4
Hydraulic fracture permeability (mD)	10000
Matrix porosity (-)	0.092
Hydraulic fracture opening (mm)	10
Formation thickness (m)	15
Matrix compression coefficient (MPa^{-1})	1.07×10^{-4}
Fracture compression factor (MPa^{-1})	1.07×10^{-4}
CO_2 Langmuir pressure (MPa)	8
CO_2 Langmuir volume (sm^3/m^3)	8
Stress sensitivity coefficient (1/MPa)	0.2

(7) The stress sensibility exists in the fracture system leading to permeability changing with pressure [43].

The velocity equation and flow equation based on the law of conservation of mass can be written as follows:

Matrix system:

$$v_m = -D_K \operatorname{grad} V,$$
$$\operatorname{div}(\rho_{sc} v_m) + \rho_{sc} \frac{\partial V}{\partial t} = 0. \tag{1}$$

Fracture system:

$$v_f = -\frac{3.6K_f}{\mu} \mathbf{grad}\, p,$$
$$\operatorname{div}(\rho v_f) - \rho_{scf} \frac{\partial V}{\partial t} = \frac{\partial(\rho\varphi)}{\partial t}. \tag{2}$$

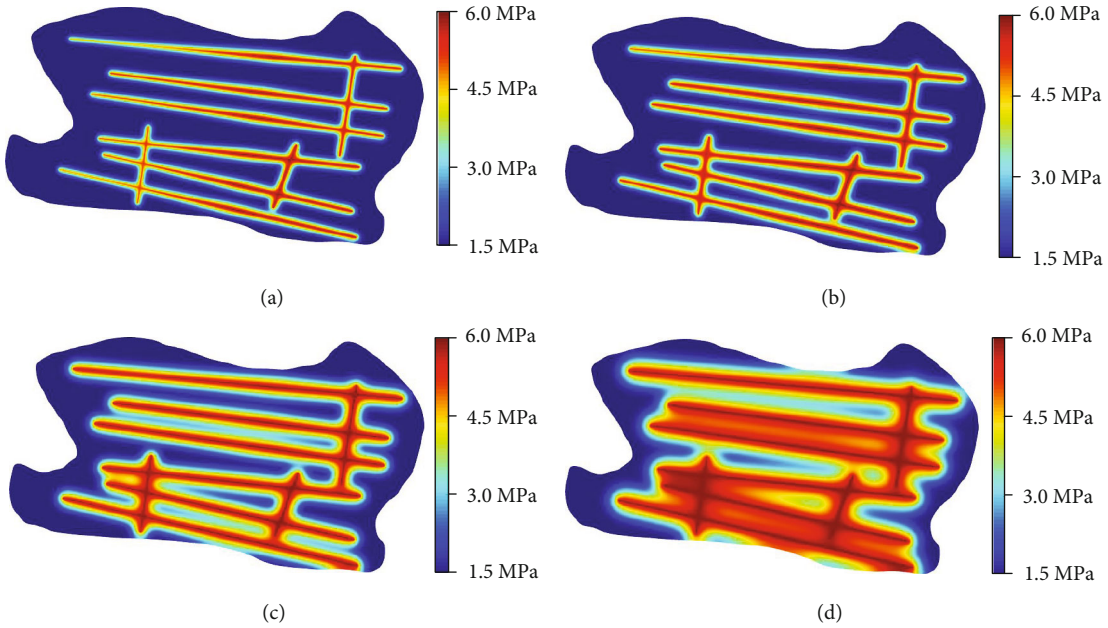

Figure 5: Pressure distribution of the system. (a) After 60 days. (b) After 90 days. (c) After 180 days. (d) After 360 days.

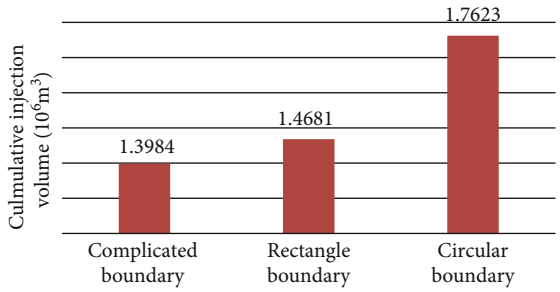

Figure 6: The cumulative CO_2 injection volume (storage volume) after 720 days.

Basic equations for CO_2 can be obtained from the following assumptions:

CO_2 adsorption equation:

$$V = V_L \frac{p}{p + p_L}. \tag{3}$$

Permeability-pressure equation

$$K_f = K_{fi} e^{-\alpha(p_i - p)}. \tag{4}$$

The flow model, which consists of the matrix system and fracture system after dimensionless transformation, can be written as follows:

Matrix system:

$$\frac{1}{{r_{mD}}^2} \frac{\partial}{\partial r_{mD}} \left({r_{mD}}^2 \frac{\partial V_D}{\partial r_{mD}} \right) = \frac{1}{D_{KD}} \frac{\partial V_D}{\partial t_D}. \tag{5}$$

The boundary condition can be written as

$$\left. \frac{\partial V_D}{\partial r_{mD}} \right|_{r_{mD} \longrightarrow 0} = 0, V_D|_{r_{mD}=1} = V_{ED}, V_D|_{t_D=0} = 0. \tag{6}$$

Fracture system:

$$\frac{\partial^2 m_{1D}}{\partial^2 r_{sD}} + \frac{2}{r_{sD}} \frac{\partial m_{1D}}{\partial r_{sD}} - \gamma_D \left(\frac{\partial m_{1D}}{\partial r_{sD}} \right)^2 = e^{\gamma_D} \left[\omega \frac{\partial m_{1D}}{\partial t_D} + (1 - \omega) \frac{\partial V_D}{\partial t_D} \right]. \tag{7}$$

The boundary condition can be written as

$$\lim_{\varepsilon_D \longrightarrow 0} 2e^{-\gamma D} {r_{sD}}^2 \left. \frac{\partial m_{1D}}{\partial r_{sD}} \right|_{r_{sD}=\varepsilon_D} = -\widehat{q}_D, m_{1D}|_{r_{sD} \longrightarrow \infty} = 0, m_{1D}|_{t_D=0} = 0. \tag{8}$$

A point source function is obtained by using Laplace transform, Pedrosa's substitution [38], and solution of the CO_2 flow model [33, 34]. Moreover, the dimensionless definitions of this article are given in the appendix.

$$\overline{G_D} = \frac{\overline{\widehat{q}_D}}{2} \frac{e^{-r_{sD}\sqrt{u}}}{r_{sD}}, \tag{9}$$

where

$$r_{sD} = \sqrt{(x_D - x_{wD})^2 + (y_D - y_{wD})^2},$$
$$u = \omega s + (1 - \omega) 3\alpha D_{KD} \left[\sqrt{s/D_{KD}} \coth \left(\sqrt{s/D_{KD}} \right) - 1 \right]. \tag{10}$$

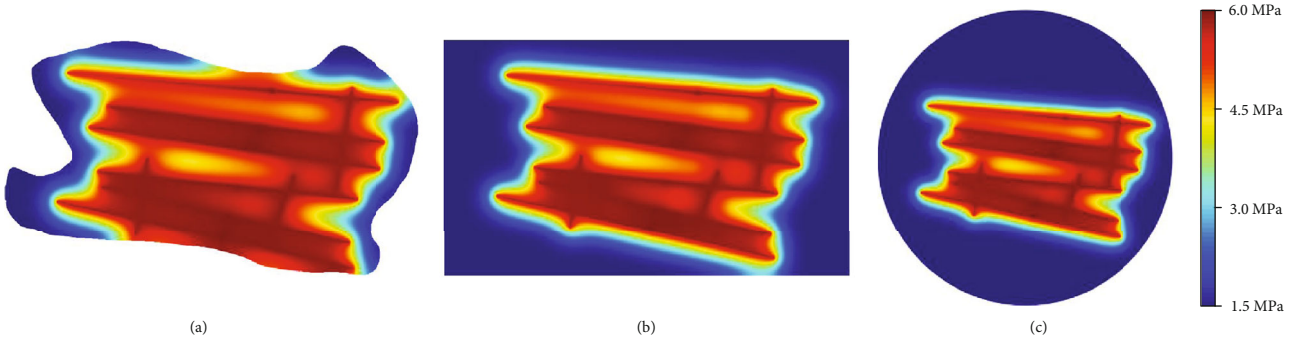

Figure 7: Pressure distribution after 720 days of injection in different boundary shapes: (a) irregular boundary shape, (b) rectangular boundary shape, and (c) circular boundary.

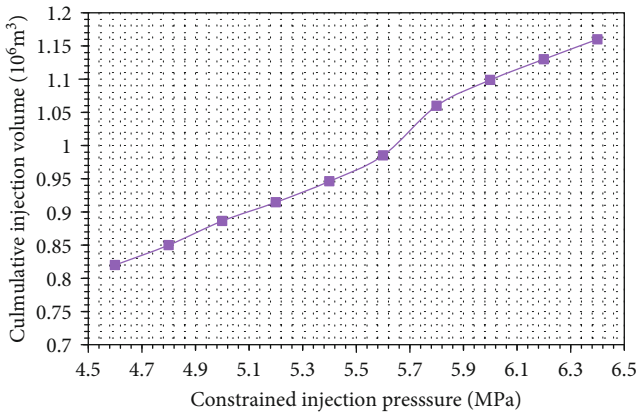

Figure 8: Cumulative injection volume under different constrained injection pressures for 360 days.

The integral equation of the dimensionless pressure using Green's secondary identity can be written as

$$\theta\bar{p}_D(x_D, y_D; s) = \int_{\Gamma_D}\left(\bar{G}_D\frac{\partial\bar{p}_D}{\partial n_D} - \bar{p}_D\frac{\partial\bar{G}_D}{\partial n_D}\right)d\Gamma + \pi\int_{\Omega_D}\bar{q}_{wD}\bar{G}_D d\Omega. \tag{11}$$

The fracture segments can be considered as point sources written as Equation (9). And then, the second term on the right side of Equation (11) can be simplified as

$$\pi\int_{\Omega_D}\bar{q}_{wD}\bar{G}_D d\Omega = \pi\sum_{j=1}^{N_F}\bar{q}_{FDj}\bar{S}_{FDj}\left(x_D, y_D, x_{wDj}, y_{wDj}, \theta_{Fj}; s\right), \tag{12}$$

where the source function for the jth segment is given by

$$\bar{S}_{FDj}\left(x_D, y_D, x_{wDj}, y_{wDj}, \theta_{Fj}; s\right) = \frac{1}{2}\Delta L_{FDj}\int_{-1}^{1}\bar{G}_D d\xi. \tag{13}$$

The boundary is divided into many boundary elements by BEM, and the number of the element on a boundary Γ is N_b, as shown in Figure 2(b). For the irregular zone, the discretized form of Equation (11) is Equation (14).

$$\theta\bar{p}_D(x_D, y_D; s) = \sum_{L=1}^{N_b}\int_{\Delta\Gamma_{DL}}\bar{G}_D\frac{\partial\bar{p}_D}{\partial n_D}d\Gamma - \sum_{L=1}^{N_b}\int_{\Delta\Gamma_{DL}}\bar{p}_D\frac{\partial\bar{G}_D}{\partial n_D}d\Gamma + \pi\sum_{j=1}^{N_F}\bar{q}_{FDj}\bar{S}_{FDj}, \tag{14}$$

where $\Delta\Gamma_{DL}$ is the Lth element on the boundary Γ_D.

The finite difference method (FDM) is used to discretize the fracture flow formula, as shown in Figure 2(a). The boundary can be discredited into N_b segments, and the fracture can be discredited into N_F segments. So $2\times N_b + 2\times N_F$ variable, including the pressure and saturation of every segment, can be solved by $2\times N_b + 2\times N_F$ equations, which consists of $N_b + N_F$ equations of the boundary condition. And N_F equations from BEM are shown as Equation (15), and N_b equations from FDM are shown as Equation (16).

$$T\bar{p}_{FD} + R\bar{q}_{FD} + \bar{p}_{wD}b = 0, \tag{15}$$

where T, R, and b are corresponding coefficient matrixes and vector, respectively.

$$A\bar{p}_D + B(\partial\bar{p}_D/\partial n_D) + C\bar{q}_{FD} = 0 \tag{16}$$

where A, B, and C are the corresponding coefficient matrixes.

The star-delta transformation is an effective method to deal with the flow of multiple adjacent fracture units. The transmissibility between the two adjacent segments with four fracture segments is given by Karimi-Fard et al. [44] and Slough et al. [45].

$$T^*_{Di,j} = \frac{\gamma_{Di}\gamma_{Dj}}{\sum_{k=1}^{4}\gamma_{Dk}}. \tag{17}$$

Assuming that another segment connected to segment 4 is labeled 5. Thus, the flow equation of segment 4 can be expressed as

$$\begin{aligned} &T^*_{D1,4}\cdot\bar{p}_{FD1} + T^*_{D2,4}\cdot\bar{p}_{FD2} + T^*_{D3,4}\cdot\bar{p}_{FD3} \\ &\quad - \left(T^*_{D1,4} + T^*_{D2,4} + T^*_{D3,4} + T_{D5,4} + \alpha_{D4}\right) \\ &\quad \cdot\bar{p}_{FD4} + T_{D5,4}\cdot\bar{p}_{FD5} - \beta_{D4}\bar{q}_{FD4} = 0, \end{aligned} \tag{18}$$

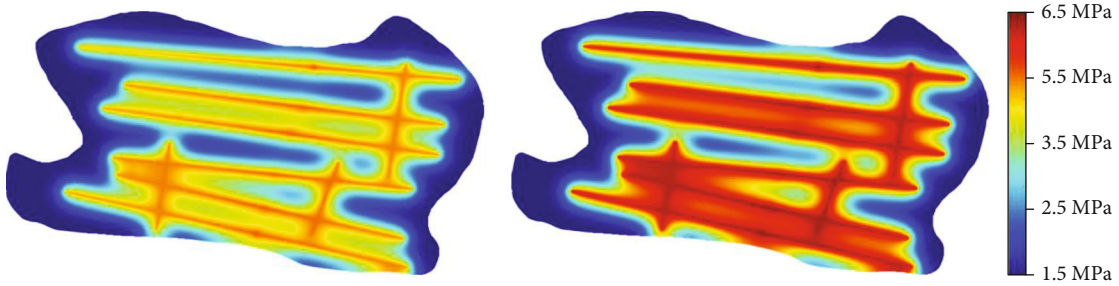

Figure 9: Pressure distribution of the system after 360 days: (a) Constrained injection pressure = 5.4 MPa and (b) constrained injection pressure = 6.4 MPa.

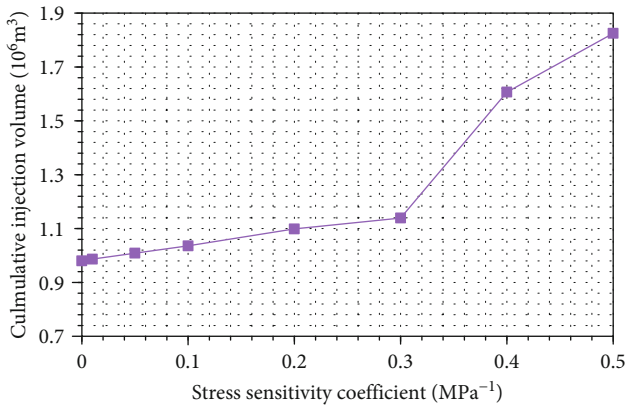

Figure 10: The cumulative injection volume of CO_2 after 360 days with different stress sensitivity coefficients.

where the transmissibility $T^*_{D1,4}$, $T^*_{D2,4}$, and $T^*_{D3,4}$ can be evaluated by use of Equation (17).

2.3. CO_2 Storage Potential Calculation. Based on the injection well transient pressure solution, the downhole pressure and the injection gas rate can be obtained. When downhole pressure reaches the target pressure, we can get the corresponding injection time t_{in}. Therefore, the CO_2 storage capacity equals the total injected CO_2 volume, which can be written as:

$$V_{in} = \int_0^{t_{in}} Q dt. \tag{19}$$

3. Verification

In this section, the developed model is validated by commercial software CMG (2012) and semianalytical models from Chen et al. [34] and Xiao et al. [24]. The parameters are shown in Table 1 and Figure 3. In total, the targeted model has a grid system of $55 * 55 * 1$, among which each grid is 50 m in the x and y directions, while it is 15 m in the z direction. The selected region covers an area of 2750×2750 m. The model validation study is conducted by comparing the cumulative injection volume under different constrained pressures, based on the same condition with regular boundary. For constant injection rate and constrained injection pressure, we compare calculated results. The new model has a high agreement with commercial software so that the new model can be regarded as an effective method, shown in Figure 4. In this case, the conventional rectangle-boundary-formation storage capacity is evaluated to verify the new method's accuracy. However, commercial software evaluation needs to use local grid refinement or irregular grid subdivision for irregular boundary reservoirs. The advantages of the new method are mainly in dealing with reservoirs with complex boundaries, without subdivision grid. The semianalytical method is adopted to evaluate the buried storage capacity according to reservoir parameters. Therefore, the semianalytical method has higher computational efficiency than the numerical simulation method.

4. Case Study

Based on an actual case from the shale gas formation, capacity evaluation is studied in this section. Furthermore, the effects of critical parameters are investigated.

4.1. Background. A depleted shale gas formation has been selected as the targeted formation, which is located in China. China has enormous development potential for shale gas, and it can be a prospective location for CO_2 storage projects to reduce greenhouse gases. The case's payzone depth ranges from 1730 m to 1745 m with a shale gas formation, and the parameters are shown in Table 2. The microseismic detection and the scale of the reservoir are shown in Figure 1.

4.2. Simulation Results. Based on this method, the CO_2 geological storage capacity can be evaluated in the actual case for the irregular boundary. After 60, 90, 180, and 360 days, the system pressure distribution is shown as Figure 5.

4.3. Effects of Boundary Shape. The innovation of the method is that it can effectively deal with the actual shale reservoir's irregular geological boundary and have faster calculation speed than the numerical solution. The boundary shape of the reservoir is usually simplified to a circular or rectangular shape. We compared the cumulative CO_2 injection under different boundary shapes. We simulated the model with regular boundary; one is a rectangular boundary with a length of 810 m and a width of 470 m, and the other is a circular boundary with a radius of 410 m. And the cumulative CO_2 injection volume after 720 days is shown in Figure 6. Pressure distribution after 720 days with different

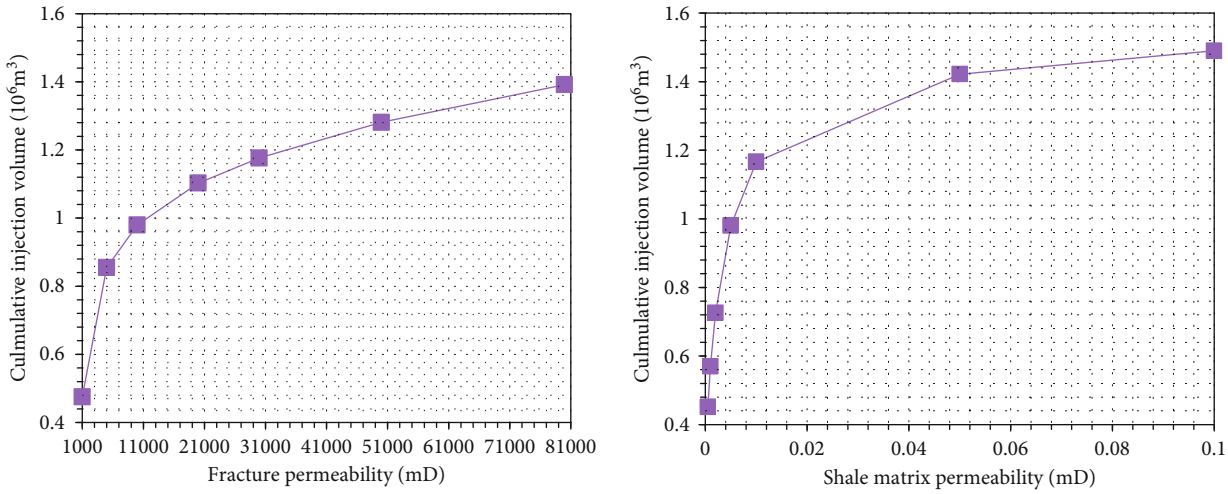

Figure 11: (a) The cumulative injection volume of CO_2 after 360 days with different fracture permeabilities. (b) The cumulative injection volume of CO_2 injected after 360 days with different matrix permeabilities.

boundary shapes under the same injection condition is shown in Figure 7. It can be seen that the shape of the reservoir boundary affects the calculation of the CO_2 storage capacity.

4.4. Sensitivity Analysis

4.4.1. Injection Pressure. Figure 8 shows the cumulative injection volume (storage volume) of CO_2 under different injection pressures. Obviously, the greater the injection pressure, the more cumulative injection amount of CO_2 (Figure 8). Figure 9 can optimize constrained injection pressure of CO_2 storage.

4.4.2. Stress Sensitivity Coefficient. Figure 10 shows the cumulative injection volume of CO_2 after 360 days under different stress sensitivity coefficients. It can be seen that the increase of fracture permeability caused by stress sensitivity has a significant influence on shale storage potential, especially when a is greater than 0.3. Therefore, the premise of accurately evaluating the CO_2 storage potential of shale reservoirs correctly considers and characterizes stress sensitivity.

4.4.3. Fracture and Shale Matrix Permeability. The cumulative injection volume of CO_2 after 360 days with different fracture permeability conditions without considering stress sensitivity is shown in Figure 11(a). It can be seen from Figure 11(a) that when the fracture conductivity is minimal, the CO_2 storage potential of the reservoir is meager. With the increase of fracture conductivity, the CO_2 reservoir potential increases sharply. It then tends to be stable, indicating that we need to find abandoned wells with better fracturing effects on the one hand. On the other hand, it is not necessary to blindly seek the high conductivity of fractures. The same law is reflected in the cumulative injection volume of CO_2 injected after 360 days with different matrix permeabilities (Figure 11(b)).

CO_2 sequestration is a long-term and complex process considering not only the storage capacity of the reservoir but also the possibility of leakage after storage. It is necessary to comprehensively consider the effectiveness and safety to finding suitable CO_2 reservoirs. It should be noted that the purpose of this method is only to provide quick and effective reference for researchers.

5. Conclusions

This study appraises CO_2 geological storage potential based on the boundary element method, evaluating the storage capacity considering arbitrarily shaped boundaries. Furthermore, this paper discusses the influence of relevant parameters on the storage capacity of a horizontal well undergoing volumetric fracturing in depleted shale gas reservoirs.

(1) The evaluation results based on the boundary element method have good agreement with commercial software so that the method can be regarded as an effective method

(2) The boundary shape of the reservoir is critical to evaluate the CO_2 geological storage capacity of depleted reservoirs accurately. The method proposed in this paper can deal with any complex boundary and simulate the CO_2 storage process effectively and efficiently

(3) The CO_2 geological storage capacity under different injection pressures, stress sensitivity coefficients, fracture permeabilities, and shale matrix permeabilities were analyzed. CO_2 geological storage design optimization should be carried out to achieve maximum benefits

The main advantage of the method proposed in this paper is that it offers quick and efficient access to CO_2

sequestration-potential estimation considering the irregular boundary, which helps select wells and monitor facilities for storing CO_2 in residual depleted shale reservoirs. Of course, some complex mechanisms were ignored, which is our subsequent work.

Appendix

Dimensionless definitions for fracture flow and flow models [30, 31]:

$$
\begin{aligned}
t_D &= \frac{3.6K_{fi}t}{\mu\left(\phi c_g + \left(K_{fi}h/\left(1.842 * 10^{-3}\right)\right)\right)h^2},\\
V_D &= V - V_i, \widehat{q}_D = \frac{\widehat{q}(t)}{q_{sc}},\\
p_{FD} &= \frac{2\pi k_I h(p_i - p_F)}{q_r B\mu_I},\\
\gamma_D &= \frac{3.684 * 10^{-3} p_{sc} q_{sc} T}{K_{fi} T_{sc} h}\gamma,\\
\alpha &= \frac{3.684 * 10^{-3}\mu Z p_{sc} q_{sc} T}{K_{fi} T_{sc} h}\frac{V_L p_L}{(p_L + p)(p_L + p_i)(p + p_i)},\\
\omega &= \frac{\phi C_g}{\phi c_g + \left(K_{fi}h/\left(1.842 * 10^{-3}\right)\right)},\\
D_{KD} &= \frac{D_K\mu\left(\phi c_g + \left(K_{fi}h/\left(1.842 * 10^{-3}\right)\right)\right)h^2}{3.6K_{fi}{R_m}^2},\\
q_{FD} &= \frac{2\zeta q_F}{q_r},\\
c_{FD} &= \frac{k_F w_F}{k\zeta},\\
\eta_{FD} &= \frac{k_F \cdot (\phi c_t)}{k \cdot (\phi c_t)_F}.
\end{aligned}
\tag{A.1}
$$

Other dimensionless definitions are $x_D = x/\zeta$, $y_D = y/\zeta$, $\varepsilon_D = \varepsilon/\zeta$, $x_{wDi} = x_{wi}/\zeta$, $y_{wDi} = y_{wi}/\zeta$, $\Delta L_{DFi} = \Delta L_{Fi}/\zeta$, $r_D = r/h$, $r_{wD} = r_w/h$, $L_{fD} = L_f/h$, and .

$$
\begin{aligned}
p_D &= \frac{2\pi kh(p_i - p)}{q_r B\mu},\\
q_{wD} &= \frac{2h\zeta^2\widehat{q}_w}{q_r},\\
p_{eD} &= \frac{2\pi k_I h(p_i - p_e)}{q_r B\mu_I},\\
q_{eD} &= \frac{2\zeta q_e}{q_r}.
\end{aligned}
\tag{A.2}
$$

Nomenclature

D_k: Knudsen diffusion coefficient, $m^2\ h^{-1}$
V: CO_2 concentration, sm^3/m^3
v: CO_2 flow velocity, m/h
a: Stress sensitivity coefficient, 1/MPa
r_m: Radial distance in matrix system, m
B: Formation liquid volume factor, m^3/m^3
c_{tF}: Discrete fracture compressibility, Pa^{-1}
c_{tI}: Inner zone matrix compressibility, Pa^{-1}
c_{tO}: Outer zone matrix compressibility, Pa^{-1}
C_D: Dimensionless wellbore-storage coefficient
F_s: Storability ratio between the inner and outer zones
G: Green function for modified Helmholtz equation
h: Formation thickness, m
k_F: Discrete fracture permeability, m^2
k: Matrix permeability, m^2
M: Mobility ratio between the inner and outer zones
N_b: Number of node point of boundary Γ
p_i: Initial formation pressure, Pa
p: Matrix pressure, Pa
p_w: Wellbore pressure, Pa
q_e: Boundary pressure, m^2/s
q_F: Flux per unit length entering the fracture, m^2/s
q_r: Reference rate, m^3/s
$\widehat{q}_w$: Flow density to fracture, s^{-1}
r_w: Wellbore radius, m
s: Laplace transformation variable
S_c: Skin factor for flow choking
S_F: Source function for fracture segment
t: Time, s
α_D: Coefficient of dimensionless pressure of fracture segment
y: y-coordinate, m
y_{wi}: y-coordinate of midpoint of fracture segment i, m
w_F: Discrete fracture width, m
ΔL_{Fi}: Length of discrete fracture segment i, m
r_s: Spherical distance in natural fracture system, m
β_D: Coefficient of dimensionless flow rate of fracture segment
γ_D: Dimensionless transmissibility between the fracture segment and interface
ε: Direction of discrete fracture, m
x: Reference length in the system, m
η: Local coordinate for boundary element
θ: Angle
μ: Fluid viscosity, Pa·s
ϕ: Matrix porosity, fraction
λ: Interporosity flow parameter
Ω: SRV zone
Γ: Boundary
ρ: Density, kg/m^3
$T^*_{Di,j}$: Dimensionless transmissibility between fracture segments i and j after star-delta transformation
x: x-coordinate, m
x_{wi}: x-coordinate of midpoint of fracture segment i, m
t_D: Dimensionless time
$T_{Di,j}$:

Dimensionless transmissibility between fracture segments i and j.

Superscripts

—: Laplace transform

Subscripts

D: Dimensionless
F: Discrete fracture
i: Discrete fracture segment index
K: Boundary nodal point index
L: Boundary element index.

Data Availability

Previously reported data were used to support this study and are available. These prior studies (and datasets) are cited at relevant places within the text as references [24, 34]. And the other data used to support the findings of this study are included within the article.

Conflicts of Interest

The authors declare that they have no conflicts of interest.

Acknowledgments

We would further like to thank the financial support of the National Natural Science Foundation of China (Nos. 51774297 and U1762210). We also acknowledge that this study was partially funded by the China Petroleum Technology Project (No. ZLZX2020-02-04).

References

[1] D. Y. Leung, G. Caramanna, and M. M. Maroto-Valer, "An overview of current status of carbon dioxide capture and storage technologies," *Renewable and Sustainable Energy Reviews*, vol. 39, pp. 426–443, 2014.

[2] E. S. Rubin, J. E. Davison, and H. J. Herzog, "The cost of CO 2 capture and storage," *International Journal of Greenhouse Gas Control*, vol. 40, article S1750583615001814, 2015.

[3] S. Benson and P. Cook, "Underground geological storage," in *Special Report on Carbon Dioxide Capture and StorageCambridge University Press*, pp. 197–265, Cambridge, UK, 2006.

[4] K. Michael, A. Golab, V. Shulakova et al., "Geological storage of CO_2 in saline aquifers–a review of the experience from existing storage operations," *International Journal of Greenhouse Gas Control*, vol. 4, no. 4, pp. 659–667, 2010.

[5] S. Shoaib and B. T. Hoffman, "CO2 flooding the Elm Coulee field," in *SPE Rocky Mountain Petroleum Technology Conference*, Denver, Colorado, 2009.

[6] T. Wan, J. J. Sheng, and M. Y. Soliman, *Evaluation of the EOR Potential in Shale Oil Reservoirs by Cyclic Gas Injection, SPWLA 54th Annual Logging Symposium*, Society of Petrophysicists and Well-Log Analysts, New Orleans, Louisiana, 2013.

[7] N. Alharthy, T. Teklu, H. Kazemi et al., "Enhanced oil recovery in liquid-rich shale reservoirs: laboratory to field," *SPE Reservoir Evaluation & Engineering*, vol. 21, no. 1, pp. 137–159, 2018.

[8] S. B. Hawthorne, C. D. Gorecki, J. A. Sorensen, E. N. Steadman, J. A. Harju, and S. Melzer, "Hydrocarbon mobilization mechanisms from upper, middle, and lower Bakken reservoir rocks exposed to C.O.," in *SPE Unconventional Resources Conference Canada*, Calgary, Alberta, Canada, 2013.

[9] T. Wan, X. Meng, J. J. Sheng, and M. Watson, "Compositional modeling of EOR process in stimulated shale oil reservoirs by cyclic gas injection," in *SPE Improved Oil Recovery Symposium*, Tulsa, Oklahoma, USA, 2014.

[10] W. Pu, *EOS Modeling and Reservoir Simulation Study of Bakken Gas Injection Improved Oil Recovery in the Elm Coulee Field*, Colorado School of Mines, Montana, 2013.

[11] W. Yu, H. Lashgari, and K. Sepehrnoori, "Simulation study of CO2 huff-n-puff process in Bakken tight oil reservoirs," in *SPE Western North American and rocky mountain joint meeting*, Denver, Colorado, 2014.

[12] P. Zhu, M. T. Balhoff, and K. K. Mohanty, "Simulation of fracture-to-fracture gas injection in an oil-rich shale," in *SPE Annual Technical Conference and Exhibition*, Houston, Texas, USA, 2015.

[13] B. Jia, J.-S. Tsau, and R. Barati, "A review of the current progress of CO_2 injection EOR and carbon storage in shale oil reservoirs," *Fuel*, vol. 236, pp. 404–427, 2019.

[14] P. Zuloaga-Molero, W. Yu, Y. Xu, K. Sepehrnoori, and B. Li, "Simulation study of CO2-EOR in tight oil reservoirs with complex fracture geometries," *Scientific Reports*, vol. 6, no. 1, p. 33445, 2016.

[15] J. Sun, A. Zou, E. Sotelo, and D. Schechter, "Numerical simulation of CO_2 huff-n-puff in complex fracture networks of unconventional liquid reservoirs," *Journal of Natural Gas Science and Engineering*, vol. 31, pp. 481–492, 2016.

[16] M. D. Aminu, S. A. Nabavi, C. A. Rochelle, and V. Manovic, "A review of developments in carbon dioxide storage," *Applied Energy*, vol. 208, pp. 1389–1419, 2017.

[17] D. Q. Liu, Y. L. Li, and R. Agarwal, "Evaluation of CO2 storage in a shale gas reservoir compared to a deep saline aquifer in the Ordos Basin of China," *Energies*, vol. 13, no. 13, p. 3397, 2020.

[18] J. M. Bielicki, J. K. Langenfeld, Z. Tao, R. S. Middleton, A. H. Menefee, and A. F. Clarens, "The geospatial and economic viability of CO_2 storage in hydrocarbon depleted fractured shale formations," *International Journal of Greenhouse Gas Control*, vol. 75, pp. 8–23, 2018.

[19] R. Heller and M. Zoback, "Adsorption of methane and carbon dioxide on gas shale and pure mineral samples," *Journal of Unconventional Oil and Gas Resources*, vol. 8, pp. 14–24, 2014.

[20] J. S. Levine, I. Fukai, D. J. Soeder et al., "U.S. DOE NETL methodology for estimating the prospective CO_2 storage resource of shales at the national and regional scale," *International Journal of Greenhouse Gas Control*, vol. 51, pp. 81–94, 2016.

[21] M. Godec, G. Koperna, R. Petrusak, and A. Oudinot, "Potential for enhanced gas recovery and CO2 storage in the Marcellus Shale in the Eastern United States," *International Journal of Coal Geology*, vol. 118, pp. 95–104, 2013.

[22] A. Busch, S. Alles, Y. Gensterblum et al., "Carbon dioxide storage potential of shales," *International Journal of Greenhouse Gas Control*, vol. 2, no. 3, pp. 297–308, 2008.

[23] M. Arif, M. Lebedev, A. Barifcani, and S. Iglauer, "Influence of shale-total organic content on CO2 geo-storage potential," *Geophysical Research Letters*, vol. 44, no. 17, pp. 8769–8775, 2017.

[24] C. Xiao, L. Tian, Y. Yang, Y. Zhang, D. Gu, and S. Chen, "Comprehensive application of semi-analytical PTA and RTA to quantitatively determine abandonment pressure for CO_2 storage in depleted shale gas reservoirs," *Journal of Petroleum Science and Engineering*, vol. 146, pp. 813–831, 2016.

[25] S. M. Kang, E. Fathi, R. J. Ambrose, I. Y. Akkutlu, and R. F. Sigal, "Carbon dioxide storage capacity of organic-rich shales," *SPE Journal*, vol. 16, no. 4, pp. 842–855, 2011.

[26] S. Bachu, D. Bonijoly, J. Bradshaw et al., "Phase II, final report from the task force for review and identification of standards for CO2 storage capacity estimation," in *Carbon Sequestration Leadership Forum*, p. 43, Washington, United States, 2007.

[27] H. Tian, S. Zhang, S. Liu, and J. Chen, "Overmature shale gas storage capacity evaluation," in *International Petroleum Technology Conference. International Petroleum Technology Conference*, p. 4, Beijing, China, 2013.

[28] B. Ren and I. J. Duncan, "Reservoir simulation of carbon storage associated with CO_2 EOR in residual oil zones, San Andres formation of West Texas, Permian Basin, USA," *Energy*, vol. 167, pp. 391–401, 2019.

[29] Y. Abuov, N. Seisenbayev, and W. Lee, "CO2 storage potential in sedimentary basins of Kazakhstan," *International Journal of Greenhouse Gas Control*, vol. 103, article 103186, 2020.

[30] O. Andersen and H. M. Nilsen, "Investigating simplified modeling choices for numerical simulation of CO_2 storage with thermal effects," *International Journal of Greenhouse Gas Control*, vol. 72, pp. 49–64, 2018.

[31] H. R. Lashgari, A. Sun, T. W. Zhang, G. A. Pope, and L. W. Lake, "Evaluation of carbon dioxide storage and miscible gas EOR in shale oil reservoirs," *Fuel*, vol. 241, pp. 1223–1235, 2019.

[32] H. Liu, X. Rao, and H. Xiong, "Evaluation of CO_2 sequestration capacity in complex- boundary-shape shale gas reservoirs using projection-based embedded discrete fracture model (pEDFM)," *Fuel*, vol. 277, article 118201, 2020.

[33] Z. Chen, X. Liao, X. Zhao, X. Feng, J. Zang, and L. He, "A new analytical method based on pressure transient analysis to estimate carbon storage capacity of depleted shales: a case study," *International Journal of Greenhouse Gas Control*, vol. 42, pp. 46–58, 2015.

[34] Z. M. Chen, X. W. Liao, X. L. Zhao et al., "Appraising carbon geological storage potential in unconventional reservoirs using well-testing method: engineering parameters analysis," in *PE/AAPG Africa Energy and Technology Conference*, Nairobi City, Kenya, 2016.

[35] L. Tian, C. Xiao, Q. Xie, Y. Yang, Y. Zhang, and Y. Wang, "Quantitative determination of abandonment pressure for CO_2 storage in depleted shale gas reservoirs by free- simulator approach," *Journal of Natural Gas Science and Engineering*, vol. 36, pp. 519–539, 2016.

[36] A. Goodman, S. Sanguinito, M. Tkach et al., "Investigating the role of water on CO_2-Utica Shale interactions for carbon storage and shale gas extraction activities - evidence for pore scale alterations," *Fuel*, vol. 242, pp. 744–755, 2019.

[37] E. M. Myshakin, H. Singh, S. Sanguinito, G. Bromhal, and A. L. Goodman, "Flow regimes and storage efficiency of CO_2 injected into depleted shale reservoirs," *Fuel*, vol. 246, pp. 169–177, 2019.

[38] O. A. Pedrosa Jr., "Pressure transient response in stress-sensitive formations," in *SPE California Regional Meeting*, Oakland, California, 1986.

[39] P. Jia, M. Ma, C. Cao, L. Cheng, H. Yin, and Z. Li, "Capturing dynamic behavior of propped and unpropped fractures during flowback and early-time production of shale gas wells using a novel flow-geomechanics coupled model," *Journal of Petroleum Science and Engineering*, 2021.

[40] Y. Wu, L. Cheng, L. Ma et al., "A transient two-phase flow model for production prediction of tight gas wells with fracturing fluid-induced formation damage," *Journal of Petroleum Science and Engineering*, vol. 199, pp. 108–351, 2021.

[41] C. Peng, J. Shan, C. Yan, and K. Zhang, "Pressure response and production performance of volumetric fracturing horizontal well in shale gas reservoir based on boundary element method," *Engineering Analysis with Boundary Elements*, vol. 87, pp. 66–77, 2018.

[42] P. Jia, D. Wu, H. Yin, Z. Li, L. Cheng, and X. Ke, "A Practical Solution Model for Transient Pressure Behavior of Multistage Fractured Horizontal Wells with Finite Conductivity in Tight Oil Reservoirs," *Geofluids*, vol. 2021, pp. 1–10, 2021.

[43] Y. Wu, L. Cheng, S. Huang et al., "A practical method for production data analysis from multistage fractured horizontal wells in shale gas reservoirs," *Fuel*, vol. 186, pp. 821–829, 2016.

[44] M. Karimi-Fard, L. J. Durlofsky, and K. Aziz, "An efficient discrete fracture model applicable for general purpose reservoir simulators," in *SPE Reservoir Simulation Symposium*, Galveston, Texas, USA, 2003.

[45] K. Slough, E. Sudicky, and P. Forsyth, "Grid refinement for modeling multiphase flow in discretely fractured porous media," *Advances in Water Resources*, vol. 23, no. 3, pp. 261–269, 1999.